Life history diversity and signals of trade-offs in a large group of chloroviruses

Eva J.P. Lievens*, Irina V. Agarkova, David D. Dunigan, James L. Van Etten, and Lutz Becks

*Aquatic Ecology and Evolution Group, Limnological Institute, University of Konstanz, Mainaustraße 252, 78464 Konstanz, Germany; eva.j.lievens@gmail.com

Abstract

Life cycle traits shape viral evolution through their effects on epidemiology, their diversity, and their trade-offs. Despite their importance, characterizations of viral life history diversity are hampered by the difficulty of measuring viral phenotypes. In this study, we overcame these challenges to describe the life history diversity of the genus *Chlorovirus*, which contains lytic dsDNA viruses that infect unicellular green algae. We developed efficient methods to measure adsorption rate, depolarization probability, lysis completion probability, lysis time, burst size, specific infectivity, and mortality rate. We used these methods to quantify the life history traits of 35 chloroviruses from three host range groups (NC64A, Osy, and SAG viruses). The trait estimates varied between 5- and 75-fold across all the virus strains, with most traits varying substantially both within and across groups. We then used the largest virus group in our study, the NC64A viruses (n = 20), to look for correlations that could signal trade-offs between traits. This revealed that viruses with high depolarization probabilities also had higher burst sizes, but lower probabilities of completing lysis. We also found a strong negative correlation between growth rate and survival. Finally, we discovered biphasic or 'tailing' decay in all the chlorovirus groups. The nature and diversity of these traits have major implications for the ecology and evolutionary potential of the chloroviruses, and reinforce the importance of studying viral life histories.

Keywords

life history, phenotypic diversity, trade-offs, phycodnavirus, chlorovirus, *Chlorella*, flow virometry, one-step growth assay, persistence assay, non-linear models

Introduction

Life histories play an important role in the ecology and evolution of microbial viruses. Viral life histories encompass 'performance' traits such as adsorption rate, lysogeny probability, progeny number, and mortality rate (performance sensu DeLong et al. 2022). The values of these traits determine a virus' population dynamics and fitness (Weitz 2016), and shape its response to selection (Abedon et al. 2003, Dessau et al. 2012, Heineman and Brown 2012, Berngruber et al. 2013). Virus populations with diverse life cycle traits have more material upon which selection can act. Conversely, trade-offs between life history traits are likely to act as evolutionary constraints (Goldhill and Turner 2014, Keen 2014). Functional constraints have been found between e.g. lysis time and burst size (Wang 2006) and growth and extracellular survival (De Paepe and Taddei 2006), leading viruses to different ecological strategies (Suttle 2007). Moreover, through their effect on host mortality, the diversity and trade-offs in viral life cycles can affect entire microbial ecosystems (Suttle 2007, Record et al. 2016, Horas et al. 2018).

Despite the importance of life history traits for microbial viruses, there are not many studies that characterize their natural diversity. Measuring viral life cycle traits requires either microscopic resolution (e.g. Timm and Yin 2012, Vincent et al. 2021, DeLong et al. 2022), which is challenging, or tracking virus concentrations over time (Hiatt 1964, Hyman and Abedon 2009), which is labor-intensive when applied to multiple strains. Thus, most studies only phenotype a few viruses at a time. Many of the studies that do analyze multiple (> 3) microbial viruses investigate the phenotypic diversity within a given host species (e.g. Baudoux and Brussaard 2005, De Paepe and Taddei 2006, Stenholm et al. 2008, Frois-Moniz 2014, Kahn Mirzaei and Nilsson 2015, Zago et al. 2015, Litt and Jaroni 2017) or viral ecotype (e.g. Kukkaro and Bamford 2009, Mojica and Brussaard 2014, Jurczak-Kurek et al. 2016, Zaburlin et al. 2017, Edwards and Steward 2018), and not within a virus clade (though see Ceyssens et al. 2011). Most of these studies also focus on a subset of the life cycle traits (e.g. Baudoux and Brussaard 2005, Stenholm et al. 2008, Kukkaro and Bamford 2009, Frois-Moniz 2014, Zago et al. 2015, Jurczak-Kurek et al. 2016, Zaburlin et al. 2017, Edwards and Steward 2018). The missing information on phenotypic diversity makes it difficult to parameterize epidemiological models and predict evolutionary responses, and is particularly striking when contrasted with our growing understanding of viral genetic diversity (DeLong et al. 2022).

In this study, we quantified the life history of a large group of chloroviruses. Chloroviruses (family *Phycodnaviridae*, genus *Chlorovirus*) are dsDNA viruses that infect unicellular 'chlorella-like' green algae (Van Etten et al. 2020). They have a lytic life cycle (Fig. 1). Upon adsorption, the virus digests a hole in the host cell wall through which the host' plasma membrane and virion internal membrane

58 fuse (Thiel et al. 2010, Milrot et al. 2017, Agarkova et al. 2021). Virion-associated proteins then
59 depolarize the host's plasma membrane, allowing viral DNA and proteins to enter (Thiel et al. 2010,
60 Milrot et al. 2017) and preventing infection by other chloroviruses (mutual exclusion, Greiner et al.
61 2009). Viral DNA is replicated in or near the nucleus, packaged into capsids in the cytoplasm, and
62 eventually mature virions escape by lysis (Meints et al. 1986). Virions are large (~190 nm, Yan et al.
63 2000, Quispe et al. 2017) and have environmentally dependent decay (Van Etten et al. 1983,
64 Agarkova et al. 2014). The chloroviruses are known to vary in genome content and plaque size (Van
65 Etten et al. 1988, Rodrigues et al. 2022), but the life cycle traits have almost exclusively been
66 measured in the type strain PBCV-1 (exceptions: Van Etten et al. 1988, Greiner et al. 2009, Quispe et
67 al. 2017, Schiano di Visconte et al. 2022).

68 To better understand the diversity of chlorovirus life history traits, we developed efficient methods
69 that combine flow cytometry, classic kinetic assays, and statistical modeling. We used these
70 methods to quantify the full life cycle of 35 chlorovirus strains (adsorption, depolarization,
71 completion with lysis time and burst, and mortality; Fig. 1), including some newly identified traits
72 (e.g. the robust fraction; Fig. 1). We then compared the phenotypic diversity within and across three
73 host range groups, and tested for signals of trade-offs between traits. This is the most thorough
74 exploration of chlorovirus life histories to date, and provides rare insights into the diversity of
75 phytoplankton viruses.

76 **Methods**

77 We measured the life history traits of 35 chlorovirus strains using new versions of the classic one-
78 step growth and persistence assays. The modified assays are higher throughput and allow
79 quantification of the entire life cycle (Fig. 1); they rely on the distinction between virions and
80 infectious virions. In what follows, viruses are described as 'virions', 'depolarizing-capable virions', or
81 'infectious virions', and we use the terms 'multiplicity of particles (MOP)', 'multiplicity of adsorption
82 (MOA)', and 'multiplicity of infection (MOI)'. These terms are defined for our purposes in Table 1.

83 *Viruses, algae, and experimental conditions*

84 The genus *Chlorovirus* is divided into four virus groups, which are defined by their host range and
85 share a high degree of protein sequence similarity (≥ 92.6 %, Jeanniard et al. 2013, see also
86 Rodrigues et al. 2022). Throughout this study, we treat the group level as corresponding to the
87 species level, within which evolution can occur (though the NC64A viruses are paraphyletic, see
88 below). We used viruses from three groups: NC64A viruses, which infect the ciliate endosymbionts

89 *Chlorella variabilis* NC64A and *C. variabilis* Syngen 2-3; Only Syngen viruses (Osy viruses), which
90 replicate in *C. variabilis* Syngen 2-3 but not *C. variabilis* NC64A; and SAG viruses, which infect the
91 heliozoon endosymbiont *Chlorella heliozoae* SAG 3.83. All of the described procedures took place in
92 the type hosts (e.g. the SAG viruses were amplified and assayed in SAG 3.83).

93 The algal strains NC64A, Syngen 2-3, and SAG 3.83 were stored on agar slants at 4°C and inoculated
94 into liquid medium before use. We used a modified version of BBM (Nichols and Bold 1965), with
95 ammonium chloride substituted for sodium nitrate as a nitrogen source and twice the concentration
96 of trace element solution 4 (first used by Frickel et al. 2016). We keep the abbreviation BBM in order
97 to distinguish our medium from the enriched "MBBM" typically used in this model system (e.g. Van
98 Etten et al. 1983). Growth was on a shaker under the standard conditions (see below). The algae
99 used for the described assays were in late exponential phase (~2×10^6 algae/ml in this medium).

100 We phenotyped 20 NC64A viruses, 7 Osy viruses, and 8 SAG viruses (Table 2). These strains were
101 isolated from natural ponds or streams around the world between 1981 and 2017, and have been
102 maintained as part of a stock collection since then. Lysates were stored at 4°C. Before starting the
103 assays, we refreshed and amplified the virus stocks: 0.5 ml of the original lysate was inoculated into
104 10 ml of 2×10^6 algae/ml solution, left on a shaker under the standard conditions (see below) until
105 they lysed (24 h or 48 h), and filtered through 0.2 µm. The resulting filtrates were stored at 4°C and
106 their virion concentration was measured by flow cytometry (see below). The filtrates with
107 insufficient virion concentrations were given one more round of this amplification treatment.

108 Algal growth and virus replication took place under the 'standard conditions', which were 20°C and
109 constant light. Unless otherwise specified, 'shaker' refers to an orbital shaker with diameter 10 mm
110 and frequency 120 rpm. 'Culture plates' always refers to 96-well flat-bottomed tissue culture plates
111 (Techno Plastic Products, CH); 'deep well plates' always refers to 96-well 2.2 ml PP deep well plates
112 (VWR International, USA). Any 4°C storage was also dark storage.

113 *Virion quantification with flow cytometry*

114 To quantify virions, we used a flow cytometry protocol based on Brussaard (2004) and Wen et al.
115 (Wen et al. 2004). Our version does not require fixation and can handle up to 96 samples at a time
116 with 97-99 % repeatability (data not shown). Briefly, virus samples were mixed with SYBR Green I
117 stain (Merck, Germany) and Tris-EDTA buffer in a PCR plate, to a final volume of 150 µl and a final
118 SYBR Green concentration of 0.5 X. Depending on the expected virion concentration, 7.5 or 30 µl of
119 virus sample was used. The samples were heated to 80°C for 10 min, allowed to cool for 15 min, and
120 intact virions were counted by a flow cytometer. We use a BD FACSVerse (BD Biosciences, USA),

121 which has an automated loader and records the analyzed volume. Each sample was run for 30 s (40-
122 50 µl), and the virion population was identified based on its side scatter and green fluorescence. A
123 detailed protocol is available on protocols.io (Lievens 2022a).

124 *Modified one-step growth (mOSG) assay*

125 In a classic one-step growth assay, viruses and hosts are mixed at a given MOI and allowed to adsorb
126 for a short time. The solutions are then diluted to synchronize the infections, and the increase in
127 plaque-forming units is used to calculate the lysis time and burst size (Hyman and Abedon 2009).
128 Our modified one-step growth (mOSG) differed in two ways. First, we worked with virions, not
129 infectious virions: we inoculated based on MOP, and measured the increase in virion concentration
130 (cf. Brown and Bidle 2014). Second, we varied the MOP across replicates (cf. Brown and Bidle 2014,
131 Taylor et al. 2018). These differences allowed us to calculate the depolarization probability (d) in
132 addition to the adsorption constant (k), lysis time ($\mu_l \pm \sigma_l$), and burst size (b_d) (Fig. 1).

133 The mOSG assay is represented schematically for one virus strain in Fig. 2; a detailed protocol is
134 available on protocols.io (Lievens 2022b). We combined algae and viruses in culture plates. Each well
135 contained 0.1 ml solution with 1.5×10^7 algae/ml and either MOP 0.5, 1, 2, 5, or 10 of a given virus
136 filtrate (MOP 20 was included for a few strains where there was room on the plates). The virus
137 volumes were pipetted separately, so that the different MOPs were statistically independent.
138 Immediately after combining algae and viruses, the solutions were mixed for 15 min to induce
139 adsorption (1200 rpm on a microplate shaker with orbital diameter 1 mm). The infections were then
140 synchronized by 1,000-fold dilution into nine sets of deep well plates (2 µl solution + 1998 µl BBM).
141 The deep well plates were sealed with transparent foil and left under the standard conditions; they
142 were inverted every hour to prevent sedimentation. At time points 0, 2, 4, …, and 16 h after dilution,
143 we collected a set of deep well plates for sampling. These independent collections maximized the
144 statistical independence of the data. We also prepared one deep well plate containing a 1 : 10,000
145 dilution, whose purpose was to check for signals of secondary infection in the growth curves (not
146 shown in Fig. 2; see Supp. Fig. S1M). This plate was sampled after 16 h. Sampling was done as
147 follows: deep well plates were centrifuged for 15 min at 2000 g to separate virions from algae;
148 supernatants (containing virions) were transferred into culture plates, sealed, and stored at 4°C. The
149 virion concentration in the supernatants was quantified by flow cytometry within one week after
150 sampling.

151 We measured the concentration of free virions at each time point. For each virus strain, we modeled
152 this concentration as the sum of leftover unadsorbed virions and newly released progeny virions:
153 $$V(t) = \frac{1}{\delta} * \left(A_a * M * e^{-k*A_a*t_a} + A_a * \left(1 - e^{-d*\left(1-e^{-k*A_a*t_a}\right)*M}\right) * F\left(t; \mu_l, \sigma_l^2, \alpha\right) * b_d\right) \quad \text{(Eq. 1).}$$

$$\underbrace{\qquad\qquad}_{\textit{unadsorbed virions}} \quad \underbrace{\qquad\qquad\qquad\qquad\qquad\qquad}_{\textit{release of progeny virions}}$$

$V(t)$ is the free virion concentration at t hours after dilution, M is the MOP, and δ is the dilution factor. To model the concentration of unadsorbed virions, we assumed that there were enough binding sites available for all virions (Meints et al. 1988), that all virions were capable of adsorbing, and that virions adsorbed at a constant rate. In this case, the concentration of free virions at the end of the adsorption period is described by the adsorption constant k, the algal concentration during the adsorption period A_a, the duration of the adsorption period in minutes t_a, and the initial virion concentration $A_a * M$ (Hyman and Abedon 2009, Eq. 18.2). The release of progeny virions over time depends on the concentration of depolarized cells, the burst size per depolarized cell, and the distribution of lysis time. To model the concentration of depolarized cells at the end of the adsorption period, we assumed that adsorbed virions were randomly distributed across host cells, and that depolarizing-capable and depolarizing-incapable virions adsorbed at the same rate. The concentration is then derived from the Poisson distribution with expected number of events $d * \left(1 - e^{-k*A_a*t_a}\right) * M$, which is the depolarization probability d (i.e. the probability that a given virion is depolarizing-capable) multiplied by the MOA. Next, we considered that every depolarized cell produced b_d progeny virions, with b_d the average burst size per depolarized cell (the true burst size probably varied across cells (Delbrück 1945, Timm and Yin 2012, Lievens et al. accepted), but without single-cell information we cannot take this into account). Crucially, we assumed that b_d was unaffected by MOP. This assumption was based on the finding that depolarization leads to mutual exclusion in chloroviruses (all depolarized cells are infected by max. one virion, Greiner et al. 2009), and was supported by single-cell burst size data for a related chlorovirus (Lievens et al. accepted). Finally, under the simplification that all depolarized host cells produced b_d, the distribution of lysis time could be approximated by a truncated normal distribution. The proportion of lysed cells over time $F(t)$ is the distribution's cumulative distribution function, with mean lysis time μ_l, standard deviation σ_l, and truncation value α. We set the truncation value α to 0 for simplicity (for the majority of the virus strains, including α as a separate parameter did not improve the fit nor affect the other parameter estimates, Supp. Fig. S2). The model is derived with supporting literature in Supp. Method S1, the model parameters are summarized in Table 3, and the effects of the parameters are demonstrated graphically in Supp. Fig. S3.

For each viral strain, we fit Eq. 1 to our data using nonlinear least squares fitting ('nls' in base R version 3.6.1, R Core Team 2014). Function $F(t)$ was calculated with the 'EnvStats' package (Millard 2013). The data was *ln*-transformed and curated before fitting: obvious outliers were removed (virion concentration implausibly high or low compared to the data for other MOPs at the same time

188 point, or compared to other time points of that MOP), as were time points with secondary infections
189 (aberrant 1 : 1,000 vs. 1 : 10,000 dilutions data at time point 16 h, or secondary increases at later
190 time points for low MOPs). For the fitting, all parameters were given appropriate lower limits (0 for
191 k and d; 0.5 for σ_l; 1 for μ_l and b_d). k, μ_l, σ_l, and b_d were given unrealistically high upper limits; d
192 was given a meaningful upper limit of 1. To ensure the parameter estimates were robust, we used a
193 variety of initial parameters for each model (example in Supp. Fig. S1, panels A-D). The quality of the
194 model fit was assessed by visually judging the fit and distribution of residuals (example in Supp. Fig.
195 S1, panels I-O). Non-parametric bootstrapping was used to obtain 95 % CIs for each parameter
196 (package 'nlstools', Baty et al. 2015 p. 20) (example in Supp. Fig. S1, panels E-H).

197 We tested the repeatability of the mOSG assay in separate experiments with four MOPs (0.5, 1, 5,
198 10) and time points up to 14 h (results shown in Supp. Fig. S4). The repeatabilities of the point
199 estimates were 0.86 for k, 0.82 for d, 0.51 for μ_l, 0.44 for σ_l, and 0.65 for b_d (n = 10, 17, 8, 8, and 16
200 strains, respectively, each strain tested twice; calculated following Nakagawa and Schielzeth 2010).
201 When an effect of the testing day was included to account for environmental variation, repeatability
202 increased to 0.76 for μ_l, 0.57 for σ_l, and 0.83 for b_d. Note that we used more MOPs, more time
203 points, and a single testing day in this mOSG assay, so our power was certainly higher.

204 *Modified persistence (mP) assay*

205 A classic persistence assay (also called survival, inactivation, or decay assay) exposes a virus solution
206 to an environment and measures the decline in infectious virions over time. At each time point, the
207 concentration of infectious virions is estimated via serial dilution methods, e.g. plaque or most
208 probable number assays (e.g. Suttle and Chan 1994, De Paepe and Taddei 2006). In contrast, our
209 modified persistence (mP) assay started with solutions with known virion concentrations, allowing
210 us to estimate the initial frequency of infectious virions (*s*, the specific infectivity) as well as their
211 mortality rate (*m*) (Fig. 1). The data also supported the existence of an additional trait, the robust
212 fraction (*r*, see below) (Fig. 1).

213 We quantified the persistence of infectious virions under our standard conditions. The assay is
214 represented schematically for one virus strain in Fig. 2; a detailed protocol is available on
215 protocols.io (Lievens 2022c). First, we produced "fresh" viruses by amplifying viruses in 10 ml of
216 1×10^6 algae/ml solution. The amplification was started with a modest number of virions (~5×10^5
217 virions/ml) and incubated for 24 h on a shaker under the standard conditions. After 24 h, solutions
218 were filtered through 0.45 µm, and the virion concentration in the filtrates was immediately
219 quantified by flow cytometry. We then prepared virion solutions with different concentrations: in
220 deep well plates, we combined filtrates and BBM to produce 1.5 ml solutions containing 5×10^4,

221 5×10^3, 5×10^2, and 5×10^1 virions/ml of a given virus strain. The filtrate volumes were pipetted
222 separately, so that the different dilutions were statistically independent. The solutions were mixed
223 and aliquoted into five sets of culture plates, which were sealed with transparent foil and left under
224 the standard conditions. After 0, 7, 14, 21, and 28 days, we used a set of culture plates to measure
225 the concentration of infectious virions in each solution: 10 µl from each solution was added to 16
226 culture wells containing 190 µl of 1.05×10^6 algae/ml solution (also in culture plates). These were
227 kept on a shaker under the standard conditions for 4 days, after which we measured the OD_{680} to
228 determine which culture wells contained viable algae (virus-negative) and which did not (virus-
229 positive). Using aliquots instead of longitudinal sampling maximized the statistical independence of
230 the data.

231 We measured the number of virus-positive vs. virus-negative wells produced at each time point. For
232 each virus strain, we modeled the proportion of virus-positive wells as
233 $P(t) = 1 - e^{-(V*s*r+V*s*(1-r)*e^{-m*t})}$ (Eq. 2).
234 This is a biphasic decay model, which assumes that infectious virions can be either "fragile", i.e.
235 susceptible to decay, or "robust", i.e. immortal. We used this model because the exponential decay
236 model was a poor fit for many of our virus strains (Supp. Fig. S5, Supp. Method S1). This biphasic
237 parametrization was the simplest extension of the exponential model, and fit our data very well. In
238 the model, $P(t)$ is the proportion of virus-positive wells after t days under the standard conditions,
239 and $V * s * r + V * s * (1 - r) * e^{-m*t}$ is the expected number of infectious virions added to each
240 culture well. V is the initial number of virions (e.g. 10 µl of a 5×10^4 virions/ml solution = 500 virions),
241 s is the frequency of infectious virions when the solution is fresh, and r is the fraction of those
242 virions that is robust. The fragile infectious virions (fraction $1 - r$) decay exponentially with
243 mortality rate m. The probability that at least one infectious virion was added to a well is derived
244 from the Poisson distribution. The model is derived with supporting literature in Supp. Method S1,
245 the model parameters are summarized in Table 3, and the effects of the parameters are
246 demonstrated graphically in Supp. Fig. S6.

247 For each viral strain, we fit Eq. 2 to the data using generalized nonlinear regression models, with the
248 number of virus-positive and -negative wells as a binomial response variable (in R version 3.6.1, R
249 Core Team 2014, package 'gnlm', Swihart and Lindsey 2019). The parameters s, r, and m were
250 inverse logit-transformed to keep them in the interval [0,1] (m can be larger than 1, but in practice
251 the mortality rates were much lower). To ensure the parameter estimates were robust, we used a
252 variety of initial parameters for each model (example in Supp. Fig. S7, panels A-C). The quality of the
253 model fit was assessed by visually judging the fit and distribution of residuals (example in Supp. Fig.

254 S7, panels G-L). Parametric bootstrapping was used to obtain 95 % CIs for each parameter (example
255 in Supp. Fig. S7, panels D-F).

256 Biphasic decay was confirmed in a separate experiment, as was the consistency of the fits for s, r,
257 and m (results shown in Supp. Fig. S8).

258 *Comparison of mOSG and mP assays*

259 By comparing the results of the mOSG and mP assays, we could derive the final traits in the life cycle:
260 the probability that a depolarized cell completes the life cycle (c) and the burst size per completed
261 cell (b_c) (Fig. 1). We define "completion" as lysis with release of virions. The completion probability c
262 could be derived from the specific infectivity s and the depolarization probability d (see Fig. 1):
263 $c = s/d$ (Eq. 3).
264 We could then derive the average burst size per completed cell b_c as
265 $b_c = b_d/c$ (Eq. 4),
266 because the burst size of depolarized cells that don't complete the life cycle is 0 (see Fig. 1). The
267 bootstraps from the mOSG and mP assays were used to calculate confidence intervals for c and b_c.

268 Eq. 3 combines estimates from two experiments, and should thus be approached with caution. One
269 difference was that the filtrates used for the mOSG assay were stored at 4°C for 2-8 days before the
270 assay, and the mP assay filtrates were not. However, previous experiments showed that s is
271 unaffected by 4°C storage for at least 9 days (J. Clot & E.J.P. Lievens, unpublished data for strain
272 PBCV-1), so this difference was unlikely to affect our calculations. A second difference was that the
273 algae were centrifuged before the mOSG experiment to concentrate them. This may have affected
274 the algae's susceptibility to depolarization (i.e. d) or stability when infected (i.e. c), although
275 previous experiments did not support an effect of centrifugation on s (i.e. on $d*c$; E.J.P. Lievens &
276 M. Spagnuolo, unpublished data for strain PBCV-1). If the algae were changed by centrifugation, we
277 would expect the strains in each virus group to be affected equally. Finally, due to Covid-19
278 restrictions there was a 3-month delay between the two experiments, and we had to use separate
279 batches of the host algae. The batches were grown from the same agar slants, however, so at most
280 we could expect an environmental effect on s that affected all strains within a group.

281 *Growth assay*

282 Finally, we added a test of relative growth to the mP assay (not shown in Fig. 2), using the "fresh"
283 filtrates prepared at the start of that assay. For each viral strain, fresh filtrate was combined with the
284 appropriate alga in a culture plate (2 wells per strain), to a final volume of 0.2 ml containing
285 1×10^6 algae/ml and 2,500 or 25,000 virions/ml. The plate was put on a shaker under the standard

286 conditions for 24 h, and then centrifuged for 15 min at 2000 g to separate algae and viruses. The
287 virion concentration of the supernatants was measured by flow cytometry; the relative increase in
288 virions/ml was used as the measure of viral growth.

289 *Statistical analysis of the trait results*

290 Our statistical analyses explored the diversity of the traits and looked for potential trade-offs. The
291 analyses excluded trait estimates from incomplete assays (d, μ_l, σ_l, b_d, c, and b_c for strains that did
292 not finish growing in the mOSG assay; r and m for strains that did not decay in the mP assay),
293 estimates that were poorly fitted by the statistical model, and estimates with uninformatively broad
294 CIs (criteria: CI > 0.67 for d, s, and c; CI spanning more than an order of magnitude for b_d, r, and b_c; CI
295 overlapping with the upper fitting constraint for k, μ_l, σ_l, and m). The retained trait estimates were
296 analyzed in R version 3.6.1 (R Core Team 2014).

297 To examine the trait diversity within and among virus groups, we fit ANOVAs to each trait measured
298 in the mOSG and mP assays. First, we partitioned variance among the virus groups using the full
299 dataset (n = 20 NC64A viruses, 8 SAG viruses, 7 Osy viruses; Table 2). Second, we used the strains
300 with a known phylogenetic position to compare the variance partitioning across virus groups vs.
301 clades (n = 14 NC64A viruses, 1 Osy virus, 6 SAG viruses; Table 2). The per-clade ANOVA accounted
302 for the paraphyletic nature of the NC64A viruses, which are divided into a PBCV-1 clade and an NY-
303 2A clade by the Osy strain OSyNE-5 (Quispe et al. 2017, Rodrigues et al. 2022). For each series of
304 ANOVAs, we corrected for multiple testing with Holm's method (Holm 1979). Trait k was
305 transformed by $\times 10^9$ for computational reasons, and traits b_d, b_c, and r were *ln*-transformed to
306 normalize their distributions.

307 We also used correlational analyses to look for signals of trade-offs between the traits. This analysis
308 focused on the NC64A viruses, as they were assayed in the same algal strain. First, we looked for
309 associations between the independent life history traits (traits marked in blue in Fig. 1 plus genome
310 size, see Supp. Table 1). We tested for pairwise correlations using Spearman's rank correlations,
311 weighted by the precision of each estimate (1/√(product of the CI breadth of trait 1 and trait 2,
312 package 'weights', Pasek 2021). To ensure that weights were comparable in scale, trait k was
313 transformed by $\times 10^8$ and trait b_c was *ln*-transformed. The correlations were corrected for multiple
314 testing using Holm's method (Holm 1979). We also applied a Principal Component Analysis (PCA) to
315 the independent traits. To deal with the missing values in our dataset, we used the 'Ipca' and
316 'PairCor' methods described in Dray & Josse (2015) (Ipca from package 'missMDA', Josse and Husson
317 2016, PairCor code and biplot extension following Podani et al. 2021). Ipca uses an iterative
318 algorithm to impute missing values, while PairCor uses a pairwise correlation approach to avoid

319 missing values. If the two missing value methods produced inconsistent results, we considered that
320 the PCA was not robust. Trait k was transformed by $\times 10^8$ for computational reasons, and trait b_c
321 was *ln*-transformed to linearize it. Second, we tested for specific constraints that have been found or
322 suggested in the literature (listed in Table 4). As above, we used weighted Spearman's rank
323 correlations and corrected for multiple testing using Holm's method.

324 As trade-offs can be masked by quality effects in correlational analyses (Stearns 1989), we repeated
325 the analyses in the previous paragraph with the 'highest quality' NC64A viruses. Our proxy for
326 quality was the relative growth of the viruses in the growth assay. The only methodological
327 differences were the linearizing transformations for the PCA: trait b_c was not *ln*-transformed, and
328 trait r was logit-transformed.

329 **Results**

330 The trait estimates and their 95 % CIs are shown in the upper panels of Fig. 3. Fig. 3 does not include
331 estimates from failed or incomplete assays; estimates that were excluded as a result of poor model
332 fitting are colored red (see Supp. Table S1 for more details). Hereafter we consider only the
333 'retained' trait estimates (colored black in Fig. 3, listed in Supp. Table S1).

334 *Evaluation of model fitting*

335 Overall, Eqs. 1 and 2 fit the data well and produced reliable trait estimates. Fewer than 10 % of the
336 estimates were excluded for having uninformatively broad 95 % CIs (red in Fig. 3). The estimates'
337 precision did depend on the parameter, with the depolarization probability d and completion
338 probability c tending to have large CIs compared to the plausible phenotypic range ([0,1]). In some
339 cases, precision was probably decreased by compensating effects between parameters: the
340 bootstrapped fits revealed positive correlations between parameters μ_l & σ_l, μ_l & b_d, σ_l & b_l, and s &
341 m, and negative correlations between parameters d & b_d and s & r (Supp. Fig. S9). These effects were
342 small compared to the scale of phenotypic variation, however, so they did not prevent the models
343 from making useful distinctions between parameters (Supp. Fig. S10). An exception occurred in the
344 subset of viral strains with $s > 0.05$: in this subset the fitting variability of s & m and s & r was on the
345 same scale as the phenotypic variability, so their correlated fits are likely to confound further
346 analyses (Supp. Fig. S10C&F).

347 *Trait diversity within- and among chlorovirus groups*

348 The virus traits were remarkably diverse. There was a 5- to 75-fold variation in retained estimates for
349 every trait, and the trait ranges often overlapped between chlorovirus groups (Fig. 3, lower panels).
350 To investigate this further, we partitioned the trait variance within and among groups using ANOVAs.

351 First, we partitioned variance among the virus groups (NC64A viruses, SAG viruses, and Osy viruses)
352 using the full dataset (Supp. Table S2). Group explained a significant proportion of the variance for
353 the adsorption constant k, the mean lysis time μ_l, the SD of lysis time σ_l, and the burst size per
354 depolarized cell b_d (proportions respectively 0.33, 0.86, 0.69, 0.57; p respectively 0.01, < 0.0001,
355 < 0.0001, < 0.01).

356 Among the viruses with a known phylogenetic position, the per-group (NC64A viruses, SAG viruses,
357 and Osy viruses) and per-clade (PBCV-1 clade, NY-2A clade, SAG clade, and OSy clade) ANOVAs
358 yielded similar variance partitioning results (Supp. Table S2). There were two notable exceptions:
359 clade explained four times more of the variance in specific infectivity s (0.45 vs. 0.11 per group) and
360 twelve times more of the variance in mortality rate m (0.37 vs. 0.03). These effects were due to the
361 higher s and m values in the PBCV-1 clade compared to the NY-2A clade. Clade also explained more
362 of the variance in burst size per completed cell b_c (0.09 vs. 0.001), but this difference is unreliable
363 due to the many missing values in the NY-2A clade. Only the mean lysis time μ_l and the SD of lysis
364 time σ_l varied significantly by group or clade (p respectively < 0.0001 and < 0.01).

365 It should be noted that these analyses could not distinguish between an effect of the group (i.e. the
366 type host) and an effect of relatedness (phylogenetic dependence, Garland et al. 1993). Indeed,
367 when the "known phylogenetic position" ANOVAs were rerun as phylogenetic ANOVAs, none of the
368 group effects were statistically significant (data not shown).

369 *Correlations between traits in the NC64A viruses*

370 Correlations between life cycle traits can suggest the existence of constraints or life history
371 strategies. We used our largest virus group, the NC64A viruses, to look for such associations.

372 First, we analyzed the associations among independent traits (traits marked in blue in Fig. 1 plus
373 genome size). Only three pairwise correlations were statistically significant (Fig. 4A and Supp. Fig.
374 S11, Supp. Table S3): the burst size per completed cell b_c and depolarization probability d were
375 negatively correlated with the completion probability c (resp. ρ = -0.89 and -0.84, p = 0.002 and 0.01)
376 and positively correlated with each other (ρ = 0.87, p = 0.002). When this dataset was used for PCA,
377 the PairCor and Ipca methods were inconsistent (data not shown), so these PCA results are not
378 interpreted further.

379 Second, we looked for additional correlations that we specifically hypothesized might occur (Fig. 4B
380 and Supp. Fig. S11, Supp. Table S3). Short-term virion quality (represented by the specific infectivity
381 s) was significantly correlated with long-term virion quality in the form of mortality rate m ($\rho = 0.83$,
382 $p = 0.0003$), but not in the form of the robust fraction r. Survival (represented by the mortality rate
383 m) was significantly correlated with reproduction in the form of relative growth ($\rho = 0.76$, $p = 0.002$),
384 but not with the 'multiplication rate' as in De Paepe & Taddei (2006). Finally, offspring quantity
385 (burst size per infected cell b_d) and quality (represented by the specific infectivity s) were not
386 significantly correlated.

387 *Correlations between traits in the fastest-growing NC64A viruses*

388 Because overall quality can confound the detection of constraints (Stearns 1989), we repeated the
389 analyses from the previous section on the 12 fastest-growing NC64A viruses. These were: AN69C,
390 CA-4A, CV-K1, CvsA1, IL-3A, IL-5-2s1, MA-1E, NE-JV-4, NYs-1, PBCV-1, WNE-10B-L2, and XZ-4A (see
391 Fig. 4C, Supp. Table S1).

392 For most pairwise comparisons of independent traits, the correlation coefficients were similar for
393 the restricted and full datasets (Fig. 5A, Supp. Table S3). However, only the positive correlation
394 between the burst size per completed cell b_c and depolarization probability d remained significant in
395 the restricted dataset ($\rho = 0.86$, $p = 0.02$). The PCAs of the independent traits were robust to the
396 missing-value method. They supported the association between burst size per completed cell b_c,
397 depolarization probability d, and completion probability c, and associated this axis with the
398 adsorption constant k (Fig. 5B). The mean and SD of lysis time μ_l and σ_l were positively associated,
399 and mortality rate m was negatively associated with the robust fraction r.

400 None of the additional correlations were significant in the fastest-growing NC64A viruses, and the
401 positive correlation between relative growth and mortality rate m was lost (Fig. 5C, Supp. Table S3).
402 As all the fastest-growing strains had specific infectivity $s > 0.05$, we did not consider the correlations
403 between s and mortality rate m or robust fraction r (see above & Supp. Fig. S10C&F).

404 **Discussion**

405 Viral life histories shape their epidemiology, ecosystem effects, and evolutionary potential. In this
406 study, we modified classic methods to quantify the life cycle traits of 35 chloroviruses from the
407 NC64A, Osy, and SAG virus groups. We found high trait diversity among these viruses, with evidence

408 for trade-offs between some traits (summarized in Fig. 6). We discuss these findings below, and also
409 highlight new insights into the chlorovirus life cycle.

410 The traits we measured included genome, virion, and virocell performance traits (sensu DeLong et al.
411 2022); we focus on their performance aspects here. The virion and virocell phenotypes were
412 probably mediated by interactions between the viral genotype, the host genotype, and the
413 environment (G_V x G_H x E interactions), which should be kept in mind when comparing traits
414 between groups and with other studies.

415 *High trait diversity within and across chlorovirus groups*

416 The first goal of our study was to explore the trait diversity of the chloroviruses, which influences
417 their evolvability and the range of their ecological effects. The strains we used were known to vary in
418 genome size and plaque size (Supp. Table S1). We can now add that they vary substantially in every
419 life cycle trait, both within and between virus groups (Fig. 3).

420 We can assume that the within-group diversity in chlorovirus traits is a consequence of genetic
421 variation, as the strains were tested in the same host and environment (G_H and E kept constant). This
422 genetic association would allow an evolutionary response to occur if selection favors a particular
423 phenotype, which may happen during the progression of an epidemic (Frank 1996, Bolker et al.
424 2010, Berngruber et al. 2013), as host densities change (Abedon et al. 2003, Heineman and Bull
425 2007), or in response to abiotic changes (Alizon et al. 2009, Dessau et al. 2012, Heineman and Brown
426 2012). The occurrence of chlorovirus evolution in nature is supported by work on NC64A, Osy, and
427 SAG viruses in natural ponds (Quispe et al. 2016), which showed that the frequencies of plaque size
428 phenotypes varied over the course of a year. Combining trait data with genomic data (e.g. Jeanniard
429 et al. 2013, Rodrigues et al. 2022) could allow the creation of a genotype-to-phenotype map to
430 further explore chlorovirus evolution (DeLong et al. 2022).

431 Attributing the between-group variation to genetic differences is more difficult, as the viruses were
432 not tested on a common host (only E kept constant). It is intriguing, however, that the SAG viruses
433 had shorter lysis times and slower adsorption. The SAG viruses infect *C. heliozoae*, which forms
434 symbioses with the heliozoan *Acanthocystis turfacea*, while the NC64A and Osy viruses infect *C.*
435 *variabilis*, which symbioses with the ciliate *Paramecium bursaria* (Van Etten et al. 2020). Predation of
436 the ciliate host is known to affect Osy-NE-ZA1 growth (DeLong et al. 2016, 2018, Al-Ameeli et al.
437 2021), and it is possible that chlorovirus traits respond to the broader ecological context of the
438 heliozoan or ciliate hosts.

439 The natural phenotypic diversity is likely to be even higher than the 5- to 75-fold range we
440 measured. Previous work has shown that the expression of chlorovirus traits depends on the host
441 genotype (G_H effects Quispe et al. 2017) and on environmental (E) effects such as light conditions
442 (Van Etten et al. 1983, I.V. Agarkova unpublished data), temperature (Horas et al. 2018, I.V.
443 Agarkova unpublished data), nutrient ratios (Clasen and Elser 2007, Cheng et al. 2015), and the
444 host's growth phase (Van Etten et al. 1983, E.J.P. Lievens unpublished data). It is likely that these
445 effects interact with virus strain (G_V x G_H and G_V x E effects) and with each other (G_H x E and
446 G_V x G_H x E effects), further enriching the overall phenotypic diversity. Interestingly, the relative lysis
447 times we found corresponded well to previous studies of multiple chloroviruses, but the relative
448 burst sizes did not (Supp. Table S1, Van Etten et al. 1988, Schiano di Visconte et al. 2022). This
449 suggests that different traits have different G_V x E effects, as found in other host-parasite systems
450 (Hall et al. 2017). Future research could examine the extent and functional basis of this (lack of)
451 plasticity.

452 *Evidence for constraints and life history strategies in the NC64A viruses*

453 We used our largest virus group, the NC64A viruses, to look for trait correlations that could suggest
454 the existence of trade-offs among life cycle traits (summarized in Fig. 6). While correlations cannot
455 prove or disprove that a functional constraint exists (Stearns 1989, Zera and Harshman 2001,
456 Agrawal et al. 2010), they are an important explorative step and allow comparisons with the existing
457 literature.

458 Among the independent life cycle traits, we found that virus strains with higher depolarization
459 probabilities (d) also had higher burst sizes per completed cell (b_c) and lower completion
460 probabilities (c). This three-trait association was detectable across the NC64A viruses and in the
461 high-quality subset (Fig. 4A, non-significant in Fig. 5A&B). It arises primarily from the low variation in
462 specific infectivity s and the positive correlation between d and b_d (Supp. Fig. S12). The association is
463 not counteracted by the broad confidence intervals around d and c, and is further supported by the
464 SAG viruses (Supp. Figs. S11 & S12). It is unclear why depolarization and the number of progeny
465 should come at the expense of completion. If this is a trade-off, the production of many
466 depolarizing-capable virions could be more error-prone or overly demanding on host resources. The
467 relationship with the adsorption constant k in the fastest-growing NC64A viruses (Fig. 5B) could fit
468 both possible explanations, assuming that well-adsorbing virions are more complicated or resource-
469 intensive to produce.

470 There were no other significant correlations between the independent traits. In particular, there was
471 no relationship between the mean lysis time μ_l and burst size per completed cell b_c, which has been

472 suggested as a general trade-off for lytic viruses (Goldhill and Turner 2014). Replacing b_c with the
473 infectious burst size ($s*b_c$) or nucleotide production per completed cell (genome size*b_c) did not
474 produce correlations with μ_l either (data not shown). The one-dimensional trade-off between lysis
475 time and burst size may be obscured by the comparative nature of the analysis, or it may not exist
476 for the NC64A viruses.

477 A clear pattern emerged, however, from the additional correlations: viruses with a lower long-term
478 success (higher mortality rate *m*) had a higher short-term success (higher specific infectivity *s* and
479 relative growth, Fig. 4B). These correlations were driven by the slowest-growing strains, which all
480 belonged to the NY-2A clade (AR158, MA-1D, NY-2A, NY-2B, Supp. Table S1). This finding could
481 reflect a trade-off between survival and growth, as found in phages (Table 4; correlations: De Paepe
482 and Taddei 2006, Dessau et al. 2012, confirmed trade-offs: Heineman and Brown 2012, García-
483 Villada and Drake 2013), with an extreme survival strategy evolving in the NY-2A clade. Observations
484 of the short- and long-term success of chloroviruses under more natural conditions would be
485 necessary to support this possibility. The occurrence of very slow-growing strains in the NY-2A clade
486 could also reflect an ecological difference, for example that these strains are best adapted to a host
487 genotype whose ecology favors very slow decay.

488 *New insights into chlorovirus life cycles: failure to depolarize vs. failure to complete*

489 Not all depolarized cells lead to completed infections (Quispe et al. 2017). Defective virions are a
490 well-known aspect of virus biology (Klasse 2015), and in chloroviruses they include empty capsids
491 and capsids with different membrane conformations (strain PBCV-1, Agarkova et al. 2014). The
492 chlorovirus' failure rate was generally high: depending on the strain, only 0.4-24 % of freshly-
493 produced virions were infectious (specific infectivity *s*, Fig. 3). Our estimates of *s* were lower than
494 those found previously, e.g. 10 % compared to 25-30 % for PBCV-1 (Van Etten et al. 1983). This
495 difference might be explained by the lower quality of the medium (Bratbak et al. 1998, cf. Tseng and
496 Myers 2014, Maat and Brussaard 2016, Bachy et al. 2018) or by a difference in sensitivity of liquid
497 culture vs. plaque assays. It is also possible that *s* was underestimated in our mP assay because wells
498 inoculated with very small numbers of infectious virions did not lyse within four days (especially
499 likely for slow-growing strains). Interestingly, we were able to separate viral failure into performance
500 traits: an inability to depolarize the host cell and an inability to complete the life cycle.

501 The depolarization probability varied widely between strains (Fig. 3). The 'depolarization' step in our
502 model actually includes three events: first, the host cell wall is digested by a conserved virion
503 protein, A561L (Agarkova et al. 2021); next, the viral and host membranes fuse, most likely due to
504 turgor pressure in the host cell (Thiel et al. 2010); finally, virion-associated K^+ channel proteins

505 depolarize the cell (Frohns et al. 2006, Thiel et al. 2010). The ability to successfully depolarize a host
506 is therefore dependent on specific, pre-packaged virion proteins (it is a virion trait, DeLong et al.
507 2022). We hypothesize that the interstrain variation in depolarization probability is caused by
508 variation in the efficiency or copy number of the A561L or K^+ channel proteins (K+ channel proteins
509 vary across strains, Frohns et al. 2006, PBCV-1 has ~60 copies of A651L, Dunigan et al. 2012).
510 Transcriptomic or proteomic studies on multiple virus strains should shed light on the underlying
511 mechanism.

512 Surprisingly, we find that an inability to complete the life cycle is the biggest hurdle for
513 chloroviruses: in all but one strain, fewer than half of the depolarized host cells produced progeny
514 virions (completion probability c = 0.01-0.42, Fig. 3). These low values may have been affected by an
515 underestimate in our measurement of the specific infectivity s (see above), which would have led to
516 an underestimate of c (and an overestimate of b_c). Alternately, they may have been biased by our
517 assumption that all virions were capable of adsorbing: if there was a "residual fraction" of non- or
518 slow-adsorbing virions (Gallet et al. 2012), the specific infectivity would actually be $s = P$(capable of
519 adsorbing)*d*c, and we would also have underestimated c (and overestimated b_c). Yet even if the
520 specific infectivity was twice as high, or half of the virions were incapable of adsorbing, the corrected
521 completion probability would fall below 50 % for most strains. Completion probability is a virocell
522 trait that depends on both host and virus (DeLong et al. 2022). If the virus effect is the most
523 important, then we expect the completion probability to reflect the proportion of virions with
524 inherent faults (Agarkova et al. 2014). Alternately, the interaction between virus and host could be
525 most important: algal cells probably vary in competence, e.g. through variation in their physiological
526 states (cf. Clasen and Elser 2007, Cheng et al. 2015) or expression of defense pathways (Rowe et al.
527 2013), and some virus strains could be more susceptible to this variation. More susceptible virus
528 strains could be evolutionarily mismatched with the host or susceptible to trade-offs with some
529 other virus trait (Goldhill and Turner 2014). As discussed above, the cost of completion probability
530 could be paid in depolarization quality or progeny number; if not, this does not invalidate the
531 possibility of a trade-off constraining completion probability.

532 *New insights into chlorovirus life cycles: biphasic persistence*

533 We discovered that many chloroviruses have biphasic or "tailing" persistence, with 0-10 % of the
534 initial infectious virions being resistant to decay in our model (robust fraction r, Fig. 1 & 3). In reality
535 these virions almost certainly would lose the ability to infect the host, but this was not detected in
536 our experiment. Biphasic decay is found in many virus species, and can be caused by several factors.
537 1) Changes in medium properties through time (Hiatt 1964). In this case we would have expected

538 the same biphasic pattern to occur across all strains, so this is not likely. 2) Adhesion to organic
539 particles (Agarkova et al. 2014, Pinon and Vialette 2018). In this case, we would expect to see a
540 larger robust fraction in the fast-growing strains, because they caused more lysis in the first step of
541 the mP assay, and thus produced more organic matter. We do not see this pattern (e.g. *r* between
542 0.1 and 5 % for the fast-growing NC64A viruses, Fig. 3). 3) Viral aggregation (Pinon and Vialette
543 2018). Chloroviruses are likely to aggregate, and different strains could vary in their tendency to do
544 so. 4) Two concurrent mortality processes causing differing degrees of damage (Koch 1960, Hiatt
545 1964, Roy et al. 1982, cf. Beck et al. 2014). If the first process (e.g. damage to the capsid) occurs
546 rapidly but leaves some probability of successful infection, and the second process (e.g. DNA
547 denaturation) occurs slowly and leads to complete inactivation, biphasic kinetics emerge. The
548 variation between strains could be due to variation in the stability of the two targets of inactivation;
549 the strains where $r = 0$ would then lack one target or have both decay at the same rate. 5) The
550 presence of a more resistant subpopulation with slower decay. These might be virions with fewer
551 production errors (Beauchemin et al. 2019), or virions with a specifically different phenotype (Hiatt
552 1964, Brouwer et al. 2017).

553 For possibilities 3-5, we could expect selection to optimize decay in response to each strain's native
554 environment. Selection could act synergistically on the mortality rate *m* and robust fraction *r* to
555 produce high vs. low-persistence types (though we don't see this pattern in the NC64A viruses, Fig.
556 4B). Alternatively, the robust fraction could reflect an adaptation to uncertainty in the environment.
557 If long-term persistence comes at a cost of short-term success (see above), then producing two
558 virion types could allow chloroviruses to profit from patches of concentrated algae (Frank 1996,
559 Berngruber et al. 2013) and to survive their seasonal environments (Long and Short 2016). In this
560 case, biphasic persistence could be a bet-hedging strategy (constant *r*) or a plastic strategy (*r* varying
561 in response to environmental cues); both types have been demonstrated for various virus traits (bet-
562 hedging: Gallet et al. 2012, Leggett et al. 2013, Erez et al. 2017, Chaturvedi et al. 2020, plasticity:
563 Bruce et al. 2021).

564 It is striking that we find biphasic decay in all the chlorovirus groups, because the existing work on
565 phytoplankton viruses typically assumes exponential decay (i.e. mortality at a constant rate; Suttle
566 and Chan 1994, Cottrell and Suttle 1995, Garza and Suttle 1998, Šulčius et al. 2015, Long and Short
567 2016, Demory et al. 2017, 2021a, 2021b). Though assuming exponential decay may be appropriate in
568 many cases, it seems unlikely that the chloroviruses are the only algal viruses with a robust fraction
569 (e.g. possible non-linearity in Tomaru et al. 2005). Finding biphasic decay in other phytoplankton
570 viruses could resolve some questions about their ecology, such as their ability to form 'seed banks'
571 that persist outside blooms (Long and Short 2016). It would also affect our understanding of aquatic

572 microbial communities and nutrient cycling, in which viral infection and decay play important roles
573 (Mojica and Brussaard 2014).

574 *Applicability of the methods and future work*

575 We hope that these methods will be useful to other virologists interested in life history traits. By
576 leveraging the distinction between MOP and MOI, the mOSG and mP assays measure more traits
577 than assays based on one or the other (e.g. Van Etten et al. 1983, Tomaru et al. 2005, Taylor et al.
578 2018). The high-throughput flow cytometry also makes them more efficient than e.g. quantification
579 through plaque assays. The assays should be applicable to any culturable lytic virus that can be
580 counted on a flow cytometer, which now includes many aquatic (Brussaard 2004) and human viruses
581 (Lippé 2018). Precision could be increased by increasing the sampling resolution, including more
582 MOPs, or replicating MOP treatments. The statistical models also can be edited to reflect life cycle
583 differences. For example, our models assume that burst size is constant because multiple infections
584 do not occur (discussed below). This is equivalent to a system where multiple infections occur, but
585 do not affect burst size. If multiple infections are possible and do affect burst size, the equations
586 could be extended to include a facilitation or competition factor. Finally, in systems where no
587 information is available, some inferences can be made from the relative amplitudes of the mOSG
588 curves. These should be related to MOP via a Poisson probability function if burst size is independent
589 of MOP (Supp. Fig. S13).

590 Further work on the chlorovirus life cycles could support or refute some aspects of our models. As
591 discussed above, we assumed there was no "residual fraction" during adsorption, and that robust
592 infectious virions never decay (Fig. 1). These are probably unrealistic assumptions, which could be
593 tested by longer studies of adsorption or persistence. We also assumed that all mOSG parameters
594 were independent of MOP. Mutual exclusion prevents coinfection in chloroviruses (Greiner et al.
595 2009), and we assumed that established infections were unaffected by other virions attaching to or
596 digesting the cell wall of the host. Our data was consistent with this assumption, but it had limited
597 power to detect deviations for d and b_d (Supp. Fig. S13). A recent study confirmed that burst size was
598 unaffected by MOP in a chlorovirus related to PBCV-1 (MOP 1 vs. 10, Lievens et al. accepted), but
599 previous work did find an effect of MOI on burst size in PBCV-1 (MOI 0.1-50, Van Etten et al. 1983). It
600 may be that these effects are restricted to very high MOPs/MOIs, when 'lysis from without' and dual
601 infection can occur (Tessman 1985, Chase et al. 1989). Future work may need to incorporate MOP-
602 dependencies, especially at higher MOPs (cf. Brown and Bidle 2014, Taylor et al. 2018).

603 **Conclusion**

604 A proper understanding of the ecological impact and evolutionary potential of viruses rests on a
605 knowledge of their life cycle traits. We showed that the chloroviruses have high phenotypic diversity
606 across their entire life history, both within and across host range groups. This suggests that they are
607 evolutionarily flexible, although they may be constrained by e.g. a survival-reproduction trade-off or
608 depolarization-completion trade-off. The chloroviruses also had large variation in relative growth,
609 mortality rate, and long-term persistence capabilities, which are likely to have strong effects on their
610 ecology. These results confirm the importance of studying viral life histories, and will hopefully
611 prompt similar research into other virus clades.

612 **Acknowledgements**

613 E.J.P.L. thanks J. Pantel for feedback on the statistical modeling, J. Clot for help with the viruses, R.
614 Hermann for transferring algae during lockdown, and the University of Konstanz Young Scholar Fund
615 for material support. We acknowledge the flow cytometry centre (FlowKon) at the University of
616 Konstanz for the use of flow cytometers and the expert support in instrument usage and data
617 analysis. We also thank the editor and two anonymous reviewers for constructive feedback.

618 **Data availability**

619 Data and analyses are available at doi:10.5281/zenodo.6573770.

620 **References**

621 Abedon, S. T., P. Hyman, and C. Thomas. 2003. Experimental Examination of Bacteriophage Latent-
622 Period Evolution as a Response to Bacterial Availability. Applied and Environmental
623 Microbiology 69:7499–7506.
624 Agarkova, I., B. Hertel, X. Zhang, L. Lane, A. Tchourbanov, D. D. Dunigan, G. Thiel, M. G. Rossmann,
625 and J. L. Van Etten. 2014. Dynamic attachment of Chlorovirus PBCV-1 to *Chlorella variabilis*.
626 Virology 466–467:95–102.
627 Agarkova, I. V., L. C. Lane, D. D. Dunigan, C. F. Quispe, G. A. Duncan, E. Milrot, A. Minsky, A. Esmael,
628 J. S. Ghosh, and J. L. Van Etten. 2021. Identification of a chlorovirus PBCV-1 protein involved
629 in degrading the host cell wall during virus infection. Viruses 13:1–19.
630 Agrawal, A. A., J. K. Conner, and S. Rasmann. 2010. Tradeoffs and Negative Correlations in
631 Evolutionary Ecology. Pages 243–268 *in* M. A. Bell, W. F. Eanes, D. J. Futuyma, and J. S.
632 Levinton, editors. Evolution After Darwin: the First 150 Years. Sinauer Associates.
633 Al-Ameeli, Z. T., M. A. Al-Sammak, J. P. DeLong, S. Thomas, D. D. Dunigan, and J. L. Van Etten. 2021.
634 Catalysis of chlorovirus production by the foraging of *Bursaria truncatella* on *Paramecia*
635 *bursaria* containing endosymbiotic algae. Microbial Ecology 9:2170.
636 Alizon, S., A. Hurford, N. Mideo, and M. Van Baalen. 2009. Virulence evolution and the trade-off
637 hypothesis: history, current state of affairs and the future. Journal of Evolutionary Biology
638 22:245–59.
639 Bachy, C., C. J. Charlesworth, A. M. Chan, J. F. Finke, C. H. Wong, C. L. Wei, S. Sudek, M. L. Coleman,
640 C. A. Suttle, and A. Z. Worden. 2018. Transcriptional responses of the marine green alga

641 *Micromonas pusilla* and an infecting prasinovirus under different phosphate conditions.
642 Environmental Microbiology 20:2898–2912.
643 Baty, F., C. Ritz, S. Charles, M. Brutsche, J. Flandrois, and D.-M. M. 2015. A Toolbox for Nonlinear
644 Regression in R: The Package nlstools. Journal of Statistical Software 66:1–21.
645 Baudoux, A.-C., and C. P. D. Brussaard. 2005. Characterization of different viruses infecting the
646 marine harmful algal bloom species *Phaeocystis globosa*. Virology 341:80–90.
647 Beauchemin, C. A. A., Y.-I. Kim, Q. Yu, G. Ciaramella, and J. P. DeVincenzo. 2019. Uncovering critical
648 properties of the human respiratory syncytial virus by combining in vitro assays and in silico
649 analyses. PLoS ONE 14:e0214708.
650 Beck, S. E., R. A. Rodriguez, K. G. Linden, T. M. Hargy, T. C. Larason, and H. B. Wright. 2014.
651 Wavelength dependent UV inactivation and DNA damage of adenovirus as measured by cell
652 culture infectivity and long range quantitative PCR. Environmental Science and Technology
653 48:591–598.
654 Belshaw, R., A. Gardner, A. Rambaut, and O. G. Pybus. 2008. Pacing a small cage: mutation and RNA
655 viruses. Trends in Ecology and Evolution 23:188–193.
656 Berngruber, T. W., R. Froissart, M. Choisy, and S. Gandon. 2013. Evolution of virulence in emerging
657 epidemics. PLOS Pathogens 9:e1003209.
658 Bolker, B. M., A. Nanda, and D. Shah. 2010. Transient virulence of emerging pathogens. Journal of
659 the Royal Society Interface 7:811–822.
660 Bratbak, G., A. Jacobsen, M. Heldal, K. Nagasaki, and F. Thingstad. 1998. Virus production in
661 *Phaeocystis pouchetii* and its relation to host cell growth and nutrition. Aquatic Microbial
662 Ecology 16:1–9.
663 Brouwer, A. F., M. C. Eisenberg, J. V. Remais, P. A. Collender, R. Meza, and J. N. S. Eisenberg. 2017.
664 Modeling Biphasic Environmental Decay of Pathogens and Implications for Risk Analysis.
665 Environmental Science and Technology 51:2186–2196.
666 Brown, C. M., and K. D. Bidle. 2014. Attenuation of virus production at high multiplicities of infection
667 in *Aureococcus anophagefferens*. Virology 466–467:71–81.
668 Bruce, J. B., S. Lion, A. Buckling, E. R. Westra, and S. Gandon. 2021. Regulation of prophage induction
669 and lysogenization by phage communication systems. Current Biology 31:5046–5051.
670 Brussaard, C. P. D. 2004. Optimization of procedures for counting viruses by flow cytometry. Applied
671 and Environmental Microbiology 70:1506–1513.
672 Ceyssens, P.-J., T. Glonti, A. M. Kropinski, R. Lavigne, N. Chanishvilli, L. Kulakov, N. Lashki, M.
673 Tediashvili, and M. Merabishvili. 2011. Phenotypic and genotypic variations within a single
674 bacteriophage species. Virology Journal 8:134.
675 Chase, T. E., J. A. Nelson, D. E. Burbank, and J. L. Van Etten. 1989. Mutual Exclusion Occurs in a
676 *Chlorella*-like Green Alga Inoculated with Two Viruses. Journal of General Virology 70:1829–
677 1836.
678 Chaturvedi, S., J. Klein, N. Vardi, C. Bolovan-Fritts, M. Wolf, K. Du, L. Mlera, M. Calvert, N. J.
679 Moorman, F. Goodrum, B. Huang, and L. S. Weinberger. 2020. A molecular mechanism for
680 probabilistic bet hedging and its role in viral latency. Proceedings of the National Academy of
681 Sciences of the United States of America 117:17240–17248.
682 Cheng, Y. S., J. Labavitch, and J. S. VanderGheynst. 2015. Organic and Inorganic Nitrogen Impact
683 *Chlorella variabilis* Productivity and Host Quality for Viral Production and Cell Lysis. Applied
684 Biochemistry and Biotechnology 176:467–479.
685 Clasen, J. L., and J. J. Elser. 2007. The effect of host *Chlorella* NC64A carbon : phosphorus ratio on the

686 production of *Paramecium bursaria Chlorella* Virus-1. Freshwater Biology 52:112–122.
687 Cottrell, M. T., and C. A. Suttle. 1995. Dynamics of a lytic virus infecting the photosynthetic marine
688 picoflagellate *Micromonas pusilla*. Limnology and Oceanography 40:730–739.
689 De Paepe, M., and F. Taddei. 2006. Viruses' life history: towards a mechanistic basis of a trade-off
690 between survival and reproduction among phages. PLOS Biology 4:e193.
691 Delbrück, M. 1945. The burst size distribution in the growth of bacterial viruses (bacteriophages).
692 Journal of Bacteriology 50:131–135.
693 DeLong, J. P., Z. Al-Ameeli, G. Duncan, J. L. Van Etten, and D. D. Dunigan. 2016. Predators catalyze an
694 increase in chloroviruses by foraging on the symbiotic hosts of zoochlorellae. Proceedings of
695 the National Academy of Sciences of the United States of America 113:13780–13784.
696 DeLong, J. P., Z. Al-Ameeli, S. Lyon, J. L. Van Etten, and D. D. Dunigan. 2018. Size-dependent catalysis
697 of chlorovirus population growth by a messy feeding predator. Microbial Ecology 75:847–
698 853.
699 DeLong, J. P., M. A. Al-Sammak, Z. T. Al-Ameeli, D. D. Dunigan, K. F. Edwards, J. J. Fuhrmann, J. P.
700 Gleghorn, H. Li, K. Haramoto, A. O. Harrison, M. F. Marston, R. M. Moore, S. W. Polson, B. D.
701 Ferrell, M. E. Salsbery, C. R. Schvarcz, J. Shirazi, G. F. Steward, J. L. Van Etten, and K. E.
702 Wommack. 2022. Towards an integrative view of virus phenotypes. Nature Reviews
703 Microbiology 20:83–94.
704 Demory, D., L. Arsenieff, N. Simon, C. Six, F. Rigaut-Jalabert, D. Marie, P. Ge, E. Bigeard, S. Jacquet, A.
705 Sciandra, O. Bernard, S. Rabouille, and A.-C. Baudoux. 2017. Temperature is a key factor in
706 *Micromonas*-virus interactions. ISME Journal 11:601–612.
707 Demory, D., R. Liu, Y. Chen, F. Zhao, A. R. Coenen, Q. Zeng, and J. S. Weitz. 2021a. Linking Light-
708 Dependent Life History Traits with Population Dynamics for *Prochlorococcus* and
709 Cyanophage. mSystems 5:e00586-19.
710 Demory, D., J. S. Weitz, A.-C. Baudoux, S. Touzeau, N. Simon, S. Rabouille, A. Sciandra, and O.
711 Bernard. 2021b. A thermal trade-off between viral production and degradation drives virus-
712 phytoplankton population dynamics. Ecology Letters 24:1133–1144.
713 Dessau, M., D. Goldhill, R. L. McBride, P. E. Turner, and Y. Modis. 2012. Selective Pressure Causes an
714 RNA Virus to Trade Reproductive Fitness for Increased Structural and Thermal Stability of a
715 Viral Enzyme. PLoS Genetics 8.
716 Dray, S., and J. Josse. 2015. Principal component analysis with missing values: a comparative survey
717 of methods. Plant Ecology 216:657–667.
718 Dunigan, D. D., R. L. Cerny, A. T. Bauman, J. C. Roach, L. C. Lane, I. V. Agarkova, K. Wulser, G. M.
719 Yanai-Balser, J. R. Gurnon, J. C. Vitek, B. J. Kronschnabel, A. Jeanniard, G. Blanc, C. Upton, G.
720 A. Duncan, O. W. McClung, F. Ma, and J. L. Van Etten. 2012. *Paramecium bursaria Chlorella*
721 Virus 1 Proteome Reveals Novel Architectural and Regulatory Features of a Giant Virus.
722 Journal of Virology 86:8821–8834.
723 Edwards, K. F., and G. F. Steward. 2018. Host Traits Drive Viral Life Histories across Phytoplankton
724 Viruses. American Naturalist 191:566–581.
725 Erez, Z., I. Steinberger-Levy, M. Shamir, S. Doron, A. Stokar-Avihail, Y. Peleg, S. Melamed, A. Leavitt,
726 A. Savidor, S. Albeck, G. Amitai, and R. Sorek. 2017. Communication between viruses guides
727 lysis-lysogeny decisions. Nature 541:488–493.
728 Frank, S. A. 1996. Models of parasite virulence. Quarterly Review of Biology 71:37–78.
729 Frickel, J., M. Sieber, and L. Becks. 2016. Eco-evolutionary dynamics in a co-evolving host-virus
730 system. Ecology Letters 19:450–459.

731 Frohns, F., A. Käsmann, D. Kramer, B. Schäfer, M. Mehmel, M. Kang, J. L. Van Etten, S. Gazzarrini, A.
732 Moroni, and G. Thiel. 2006. Potassium Ion Channels of *Chlorella* Viruses Cause Rapid
733 Depolarization of Host Cells during Infection. Journal of Virology 80:2437–2444.
734 Frois-Moniz, K. 2014. Host/virus interactions in the marine cyanobacterium *Prochlorococcus*. Thesis,
735 Massachusetts Institute of Technology.
736 Furió, V., A. Moya, and R. Sanjuán. 2005. The cost of replication fidelity in an RNA virus. Proceedings
737 of the National Academy of Sciences of the United States of America 102:10233–10237.
738 Gallet, R., T. Lenormand, and I. N. Wang. 2012. Phenotypic Stochasticity Protects Lytic Bacteriophage
739 Populations From Extinction During The Bacterial Stationary Phase. Evolution 66:3485–3494.
740 García-Villada, L., and J. W. Drake. 2013. Experimental selection reveals a trade-off between
741 fecundity and lifespan in the coliphage Qß. Open Biology 3:130043.
742 Garland, T. Jr., A. W. Dickerman, C. M. Janis, and J. A. Jones. 1993. Phylogenetic analysis of
743 covariance by computer simulation. Systematic Biology 42:265–292.
744 Garza, D. R., and C. A. Suttle. 1998. The Effect of Cyanophages on the Mortality of *Synechococcus*
745 spp. and Selection for UV Resistant Viral Communities. Microbial Ecology 36:281–292.
746 Goldhill, D. H., and P. E. Turner. 2014. The evolution of life history trade-offs in viruses. Current
747 Opinion in Virology 8:79–84.
748 Greiner, T., F. Frohns, M. Kang, J. L. Van Etten, A. Käsmann, A. Moroni, B. Hertel, and G. Thiel. 2009.
749 *Chlorella* viruses prevent multiple infections by depolarizing the host membrane. Journal of
750 General Virology 90:2033–2039.
751 Hall, M. D., G. Bento, and D. Ebert. 2017. The evolutionary consequences of stepwise infection
752 processes. Trends in Ecology & Evolution 32:612–623.
753 Heineman, R. H., and S. P. Brown. 2012. Experimental Evolution of a Bacteriophage Virus Reveals the
754 Trajectory of Adaptation across a Fecundity/Longevity Trade-Off. PLoS ONE 7.
755 Heineman, R. H., and J. J. Bull. 2007. Testing optimality with experimental evolution: Lysis time in a
756 bacteriophage. Evolution 61:1695–1709.
757 Hiatt, C. W. 1964. Kinetics of the inactivation of viruses. Bacteriological Reviews 28:150–163.
758 Holm, S. 1979. A simple sequentially rejective multiple test procedure. Scandinavian Journal of
759 Statistics 6:65–70.
760 Horas, E. L., L. Theodosiou, and L. Becks. 2018. Why Are Algal Viruses Not Always Successful? Viruses
761 10:474.
762 Hyman, P., and S. T. Abedon. 2009. Practical Methods for Determining Phage Growth Parameters.
763 Pages 175–202 *in* M. R. J. Clokie and A. M. Kropinski, editors. Bacteriophages: Methods and
764 Protocols, Volume 1: Isolation, Characterization, and Interactions, vol. 401. Humana Press.
765 Jeanniard, A., D. D. Dunigan, J. R. Gurnon, I. V. Agarkova, M. Kang, J. Vitek, G. Duncan, O. W.
766 McClung, M. Larsen, J. M. Claverie, J. L. Van Etten, and G. Blanc. 2013. Towards defining the
767 chloroviruses: A genomic journey through a genus of large DNA viruses. BMC Genomics 14.
768 Josse, J., and F. Husson. 2016. missMDA: A Package for Handling Missing Values in Multivariate Data
769 Analysis. Journal of Statistical Software 70:1–31.
770 Jurczak-Kurek, A., T. Gąsior, B. Nejman-Faleńczyk, S. Bloch, A. Dydecka, G. Topka, A. Necel, M.
771 Jakubowska-Deredas, M. Narajczyk, M. Richert, A. Mieszkowska, B. Wróbel, G. Węgrzyn, and
772 A. Węgrzyn. 2016. Biodiversity of bacteriophages: Morphological and biological properties of
773 a large group of phages isolated from urban sewage. Scientific Reports 6:1–17.
774 Kahn Mirzaei, M., and A. S. Nilsson. 2015. Isolation of Phages for Phage Therapy: A Comparison of
775 Spot Tests and Efficiency of Plating Analyses for Determination of Host Range and Efficacy.

776 PloS ONE 10:e0118557.
777 Keen, E. C. 2014. Tradeoffs in bacteriophage life histories. Bacteriophage 4:e28365.
778 Klasse, P. J. 2015. Molecular Determinants of the Ratio of Inert to Infectious Virus Particles. Progress
779 in Molecular Biology and Translational Science 129:285–326.
780 Koch, G. 1960. Influence of assay conditions on infectivity of heated poliovirus. Virology 12:601–603.
781 Kukkaro, P., and D. H. Bamford. 2009. Virus–host interactions in environments with a wide range of
782 ionic strengths. Environmental Microbiology Reports 1:71–77.
783 Leggett, H. C., R. Benmayor, D. J. Hodgson, and A. Buckling. 2013. Experimental evolution of adaptive
784 phenotypic plasticity in a parasite. Current Biology 23:139–142.
785 Lievens, E. J. P. 2022a. Virion quantification by flow cytometry, without fixation or freezing.
786 dx.doi.org/10.17504/protocols.io.6qpvr6q93vmk/v1.
787 Lievens, E. J. P. 2022b. Modified one-step growth (mOSG) assay.
788 dx.doi.org/10.17504/protocols.io.4r3l2op9pv1y/v2.
789 Lievens, E. J. P. 2022c. Modified persistence (mP) assay.
790 dx.doi.org/10.17504/protocols.io.81wgb6knylpk/v2.
791 Lievens, E. J. P., M. Spagnuolo, T. Réveillon, and L. Becks. accepted. Delayed lysis time at high
792 multiplicities of particles in a chlorovirus-*Chlorella* interaction.
793 Lippé, R. 2018. Flow Virometry: A Powerful Tool To Functionally Characterize Viruses. Journal of
794 Virology 92:e01765-17.
795 Litt, P. K., and D. Jaroni. 2017. Isolation and Physiomorphological Characterization of *Escherichia coli*
796 O157:H7-Infecting Bacteriophages Recovered from Beef Cattle Operations. International
797 Journal of Microbiology 2017:e7013236.
798 Long, A. M., and S. M. Short. 2016. Seasonal determinations of algal virus decay rates reveal
799 overwintering in a temperate freshwater pond. ISME Journal 10:1602–1612.
800 Maat, D. S., and C. P. D. Brussaard. 2016. Both phosphorus- and nitrogen limitation constrain viral
801 proliferation in marine phytoplankton. Aquatic Microbial Ecology 77:87–97.
802 Meints, R. H., D. E. Burbank, J. L. Van Etten, and D. T. A. Lamport. 1988. Properties of the chlorella
803 receptor for the virus PBCV-1. Virology 164:15–21.
804 Meints, R. H., K. Lee, and J. L. Van Etten. 1986. Assembly site of the virus PBCV-1 in a *Chlorella*-like
805 green alga: ultrastructural studies. Virology 154:240–245.
806 Millard, S. P. 2013. EnvStats: An R Package for Environmental Statistics. Springer, New York.
807 Milrot, E., E. Shimoni, T. Dadosh, K. Rechav, T. Unger, J. L. Van Etten, and A. Minsky. 2017. Structural
808 studies demonstrating a bacteriophage-like replication cycle of the eukaryote-infecting
809 *Paramecium bursaria* chlorella virus-1. PLOS Pathogens 13:e1006562.
810 Mojica, K. D. A., and C. P. D. Brussaard. 2014. Factors affecting virus dynamics and microbial host–
811 virus interactions in marine environments. FEMS Microbiology Ecology 89:495–515.
812 Nakagawa, S., and H. Schielzeth. 2010. Repeatability for Gaussian and non-Gaussian data: a practical
813 guide for biologists. Biological Reviews 85:935–956.
814 Nichols, H. W., and H. C. Bold. 1965. *Trichosarcina polymorpha* Gen. et Sp. Nov. Journal of Phycology
815 1:34–38.
816 Pasek, J. 2021. weights: Weighting and Weighted Statistics, version 1.0.4.
817 Pinon, A., and M. Vialette. 2018. Survival of viruses in water. Intervirology 61:214–222.
818 Podani, J., T. Kalapos, B. Barta, and D. Schmera. 2021. Principal component analysis of incomplete
819 data – A simple solution to an old problem. Ecological Informatics 61:101235.
820 Quispe, C. F., A. Esmael, O. Sonderman, M. McQuinn, I. Agarkova, M. Battah, G. A. Duncan, D. D.

821 Dunigan, P. L. Timothy, C. DeCastro, I. Speciale, F. Ma, and J. L. Van Etten. 2017.
822 Characterization of a New Chlorovirus Type with Permissive and Non-permissive Features on
823 Phylogenetically Related Algal Strains. Virology 500:103–113.
824 Quispe, C. F., O. Sonderman, A. Seng, B. Rasmussen, G. Weber, C. Mueller, D. D. Dunigan, and J. L.
825 Van Etten. 2016. Three-year survey of abundance, prevalence and genetic diversity of
826 chlorovirus populations in a small urban lake. Archives of Virology 161:1839–1847.
827 R Core Team. 2014. R: A language and environment for statistical computing. R Foundation for
828 Statistical Computing, Vienna, Austria.
829 Record, N. R., D. Talmy, and S. Våge. 2016. Quantifying tradeoffs for marine viruses. Frontiers in
830 Marine Science 3:251.
831 Rodrigues, R. A. L., V. F. Queiroz, J. Ghosh, D. D. Dunigan, and J. L. Van Etten. 2022. Functional
832 Genomic Analyses Reveal an Open Pan-genome for the Chloroviruses and a Potential for
833 Genetic Innovation in New Isolates. Journal of Virology 96:e01367-21.
834 Rowe, J. M., D. D. Dunigan, G. Blanc, J. R. Gurnon, Y. Xia, and J. L. Van Etten. 2013. Evaluation of
835 higher plant virus resistance genes in the green alga, *Chlorella variabilis* NC64A, during the
836 early phase of infection with *Paramecium bursaria* chlorella virus-1. Virology 442:101–113.
837 Roy, D., E. S. K. Chian, and R. S. Engelbrecht. 1982. Mathematical model for enterovirus inactivation
838 by ozone. Water Research 16:667–673.
839 Schiano di Visconte, G., M. J. Allen, and A. Spicer. 2022. New Insights from the High-Resolution
840 Monitoring of Microalgae–Virus Infection Dynamics. Viruses 14:466.
841 Stearns, S. C. 1989. Trade-Offs in Life-History Evolution. Functional Ecology 3:259–268.
842 Stenholm, A. R. nnest, I. Dalsgaard, and M. Middelboe. 2008. Isolation and Characterization of
843 Bacteriophages Infecting the Fish Pathogen *Flavobacterium psychrophilum*. Applied and
844 Environmental Microbiology 74:4070–4078.
845 Šulčius, S., E. Šimoliūnas, J. Staniulis, J. Koreivienė, P. Baltrušis, R. Meškys, and R. Paškauskas. 2015.
846 Characterization of a lytic cyanophage that infects the bloom-forming cyanobacterium
847 *Aphanizomenon flos-aquae*. FEMS Microbiology Ecology 91:1–7.
848 Suttle, C. A. 2007. Marine viruses - Major players in the global ecosystem. Nature Reviews
849 Microbiology 5:801–812.
850 Suttle, C. A., and A. M. Chan. 1994. Dynamics and distribution of cyanophages and their effect on
851 marine *Synechococcus* spp. Applied and Environmental Microbiology 60:3167–3174.
852 Swihart, B., and J. Lindsey. 2019. gnlm: Generalized Nonlinear Regression Models, version 1.1.1.
853 Taylor, B. P., J. S. Weitz, C. P. D. Brussaard, and M. G. Fischer. 2018. Quantitative Infection Dynamics
854 of *Cafeteria Roenbergensis* Virus. Viruses 10:468.
855 Tessman, I. 1985. Genetic recombination of the DNA plant virus PBCV1 in a *Chlorella*-like alga.
856 Virology 145:319–322.
857 Thiel, G., A. Moroni, D. D. Dunigan, and J. L. Van Etten. 2010. Initial Events Associated with Virus
858 PBCV-1 Infection of *Chlorella* NC64A. Progress in Botany 71:169–183.
859 Timm, A., and J. Yin. 2012. Kinetics of virus production from single cells. Virology 424:11–17.
860 Tomaru, Y., H. Tanabe, S. Yamanaka, and K. Nagasaki. 2005. Effects of temperature and light on
861 stability of microalgal viruses, HaV, HcV and HcRNAV. Plankton Biology and Ecology 52:1–6.
862 Tseng, M., and J. H. Myers. 2014. The relationship between parasite fitness and host condition in an
863 insect -virus system. PLoS ONE 9:e106401.
864 Van Etten, J. L., I. V. Agarkova, and D. D. Dunigan. 2020. Chloroviruses. Viruses 12:20.
865 Van Etten, J. L., D. E. Burbank, Y. Xia, and R. H. Meints. 1983. Growth cycle of a virus, PBCV-1, that

infects *Chlorella*-like algae. Virology 126:117–125.

Van Etten, J. L., A. M. Schuster, and R. H. Meints. 1988. Viruses of eukaryotic *Chlorella*-like algae. Pages 411–428 *in* Y. Koltin and M. J. Leibowitz, editors. Viruses of Fungi and Simple Eukaryotes. Marcel Dek. New York and Basel.

Vincent, F., U. Sheyn, Z. Porat, D. Schatz, and A. Vardi. 2021. Visualizing active viral infection reveals diverse cell fates in synchronized algal bloom demise. Proceedings of the National Academy of Sciences of the United States of America 118:e2021586118.

Wang, I.-N. 2006. Lysis Timing and Bacteriophage Fitness. Genetics 172:17–26.

Weitz, J. 2016. Quantitative Viral Ecology: Dynamics of Viruses and Their Microbial Hosts. Princeton University Press.

Wen, K., A. C. Ortmann, and C. A. Suttle. 2004. Accurate estimation of viral abundance by epifluorescence microscopy. Applied and Environmental Microbiology 70:3862–3867.

Yan, X., N. H. Olson, J. L. Van Etten, M. Bergoin, M. G. Rossmann, and T. S. Baker. 2000. Structure and assembly of large lipid-containing dsDNA viruses. Nature Structural Biology 7:101–103.

Zaburlin, D., A. Quiberoni, and D. Mercanti. 2017. Changes in Environmental Conditions Modify Infection Kinetics of Dairy Phages. Food and Environmental Virology 9:270–276.

Zago, M., B. Bonvini, L. Rossetti, A. Meucci, G. Giraffa, and D. Carminati. 2015. Biodiversity of *Lactobacillus helveticus* bacteriophages isolated from cheese whey starters. Journal of Dairy Research 82:242–247.

Zera, A. J., and L. G. Harshman. 2001. The Physiology of Life History Trade-Offs in Animals. Annual Review of Ecological Systems 32:95–126.

889 **Tables**

890 **Table 1. Definitions used in this paper.**

Term	Our definition	Ratio to host cells
Virions	Virus particles that can be detected by flow cytometry (excludes e.g.DNA-free capsids[1]).	Multiplicity of particles (MOP)
Adsorbed virions	Virions that are adsorbed to a host cell. Virions that have not adsorbed may be incapable or may have failed to adsorb by chance.	Multiplicity of adsorption (MOA)[2]
Depolarizing-capable virions	Virions that can depolarize a host cell if they adsorb to one. We assume that chance plays no role in depolarization success: failure to depolarize after adsorption is always due to incapability or mutual exclusion (the cell has already been depolarized by another depolarizing-capable virion[3]).	-
Infectious virions	Virions that can catalyze the death of an algal population, i.e. finish a life cycle and spread to other cells. Non-infectious virions can be incapable of adsorbing, depolarizing the host[1,4], or completing the infection[5].	Multiplicity of infection (MOI)

891 [1](Agarkova et al. 2014), [2](Hyman and Abedon 2009), [3](Greiner et al. 2009), [4](Frohns et al. 2006), [5](Quispe et al.
892 2017)

893 **Table 2. List of viral strains.** We used two lysates of reference strain AR158; lysate AR158[1] was seven
894 years older than AR158[2]. Phylogenetic positions based on Quispe et al. (2017) and Rodrigues et al.
895 (2022).

Group	Clade	Strains
NC64A viruses	PBCV-1 clade	AN69C, CV-K1 (= CviKI), CvsA1, IL-3A, KS-1B, MA-1E, NE-JV-4, PBCV-1
	NY-2A clade	AR158[1], AR158[2], IL-5-2s1, MA-1D, NY-2A, NY-2B, NYs-1
	unknown	CA-4A, SH-6A, WNE-10B-L2, WNE-11A-L2 (= WNE-11A-L1), XZ-4A
Osy viruses	Osy clade	OSyNE-5
	unknown	OSyNE-4B-L2, OSyNE-4B-M2, OSyNE-4B-S2, OSyNE-5B-M2, OSyNE-5B-S1, OSyNE-ZA-1
SAG viruses	SAG clade	Canal-1, GM0701.1, MN0810.1, MO0605SPH, NTS-1, TN603.4.2
	unknown	NES-4A-S1, NES-5A-L1

896

897 **Table 3. List of life history traits.**

Model	Parameter	Trait
Eq. 1	k	adsorption constant[1]
Eq. 1	d	depolarization probability (probability that a virion is depolarizing-capable)
Eq. 3	c	completion probability (probability that a depolarized cell will lyse and produce progeny virions)
Eq. 1	α (set to 0)	truncation value of lysis time (earliest possible lysis time)
Eq. 1	μ_l	mean lysis time
Eq. 1	σ_l	standard deviation of lysis time
Eq. 1	b_d	average burst size per depolarized cell
Eq. 4	b_c	average burst size per completed cell
Eq. 2	s	specific infectivity (proportion of virions that are infectious when the solution is fresh)
Eq. 2	r	robust fraction (fraction of initially infectious virions that do not decay)
Eq. 2	m	mortality rate of the fragile infectious virions

898 [1](Hyman and Abedon 2009)

899 **Table 4. Additional correlations that we hypothesized could occur between traits, based on trade-**
900 **offs found in or suggested by the literature.**

Trade-off	Expected correlations	Basis
Short-term vs. long-term virion quality	- specific infectivity *s* positively correlated with mortality rate *m* - specific infectivity *s* negatively correlated with the robust fraction *r*	Reflection of the general expectation that trade-offs occur between adaptations to different environments[1], in this case short-term and long-term outside-host conditions.
Survival vs. reproduction	- mortality rate *m* positively correlated with multiplication rate, calculated as b_c*s/μ_l following De Paepe & Taddei[2] - mortality rate *m* positively correlated with relative growth in the growth assay	Classic trade-off[3] that is also expected to apply to viruses[4,5]. Seminal example in De Paepe & Taddei[2].
Offspring quantity & quality	- burst size per infected cell b_d negatively correlated with specific infectivity *s*	Version of the classic quantity/quality trade-off[3,5], but at $t = 0$. Related to the speed-fidelity trade-off[6,7], though other processes than mutation may cause defective virions.

901 [1](Agrawal et al. 2010), [2](De Paepe and Taddei 2006), [3](Stearns 1989), [4](Goldhill and Turner 2014), [5](Keen 2014)
902 [6](Furió et al. 2005), [7](Belshaw et al. 2008)
903

904 **Figures**

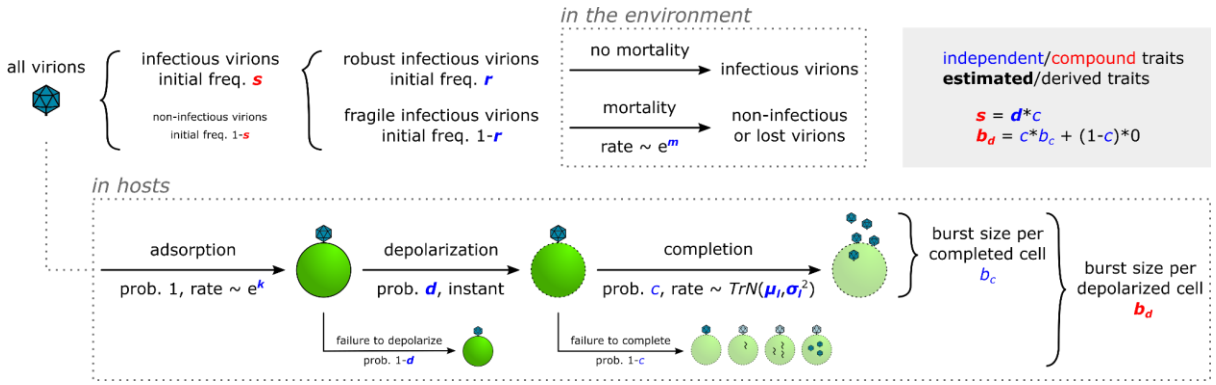

905

906 **Fig. 1. Life cycle of the chloroviruses, as assumed in our statistical models.** See the text and Table 3
907 for definitions of the traits and model assumptions. Traits marked in blue are assumed to be
908 independent of each other; traits marked in red arise from combinations of two or more other traits
909 (see gray box). Traits in bold are estimated from the modified one-step growth (mOSG) or modified
910 persistence (mP) assay results; traits not in bold are derived from comparing the two assays. "*TrN*":
911 truncated normal distribution (truncated at 0 h).

912

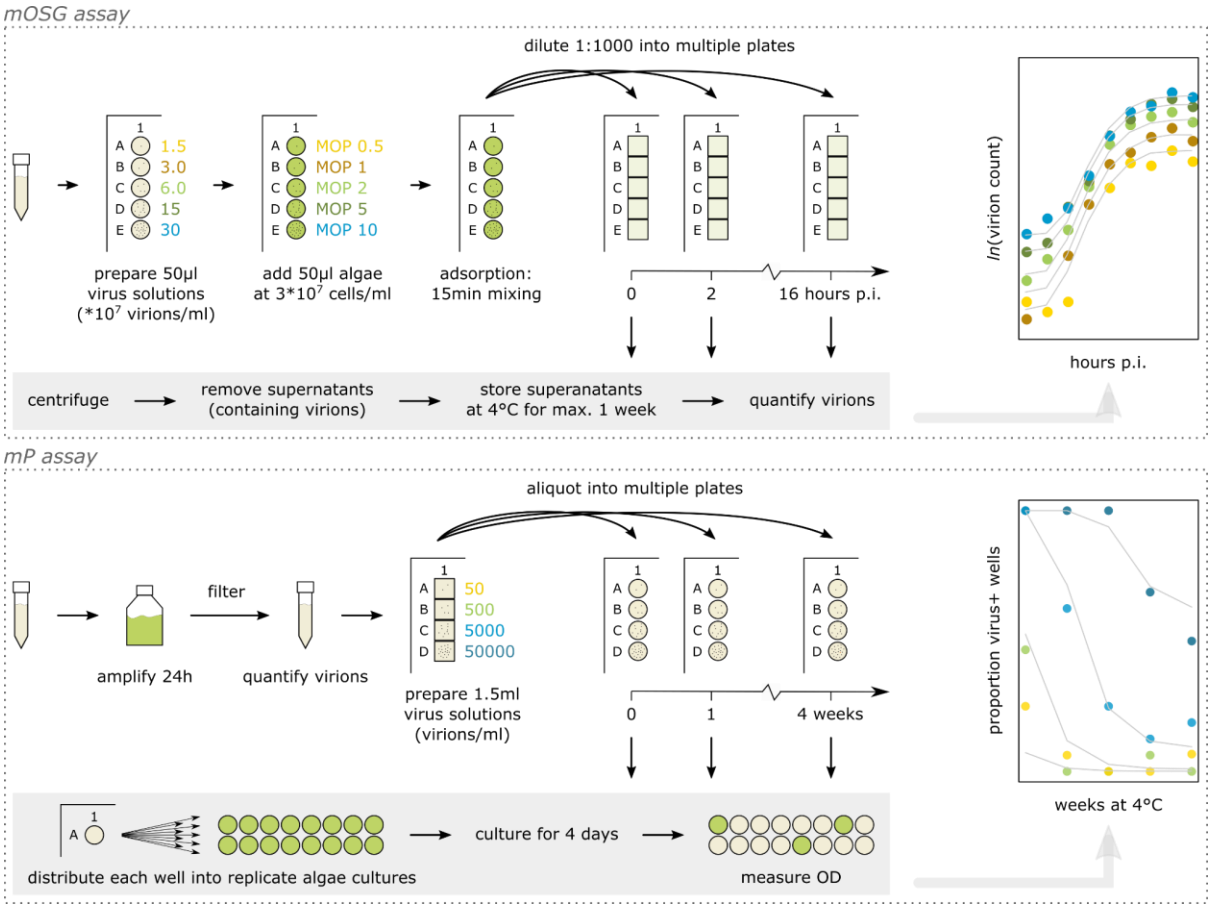

Fig. 2. Schematic representation of the mOSG and mP assays for one virus strain. Both assays started from the same filtrate, represented by a 15 ml tube. Culture plates are depicted with round wells; deep well plates with square wells. The solid gray boxes describe the sampling procedure that was repeated at every time point. On the right, the gray arrows lead to examples of the data (points) and the model fits (gray lines). The data shown here is for virus strain SH-6A.

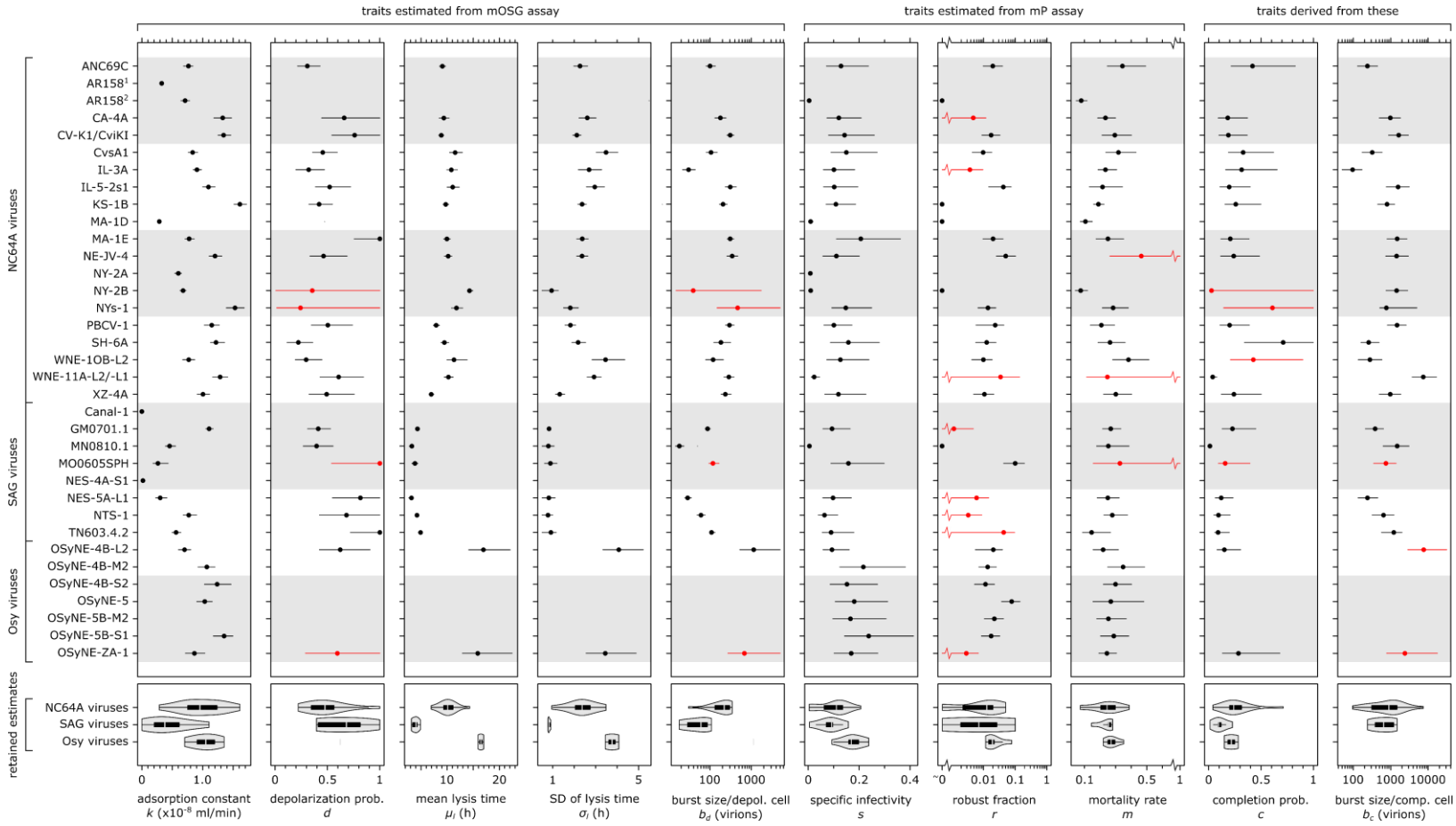

Fig. 3. Within- and across-group trait diversity revealed by the mOSG and mP assays. Upper panels: Trait estimates and 95 % CIs. Estimates and CIs colored in black were retained for further analysis; estimates and traits colored red were excluded from the analyses due to poor or imprecise model fit. Missing traits are due to failed or incomplete assays. See Supp. Table S1 for details and exact values. **Lower panels: Distributions of the retained estimates.** Shown as violin plots with internal box plots. Only the estimates used in the analyses are included in these distributions (i.e. those shown in black in the upper panels).

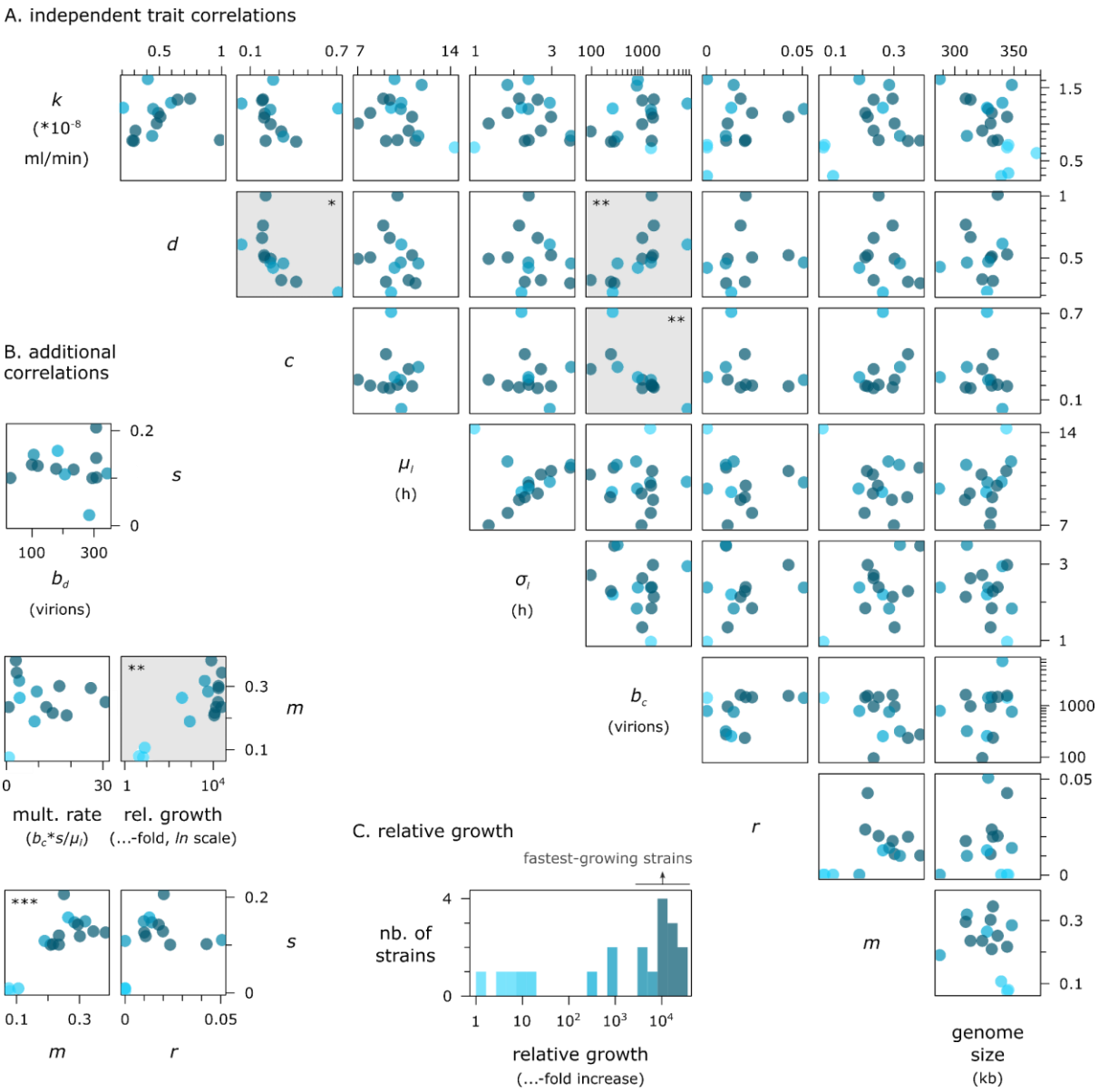

Fig. 4. Correlations between traits in the NC64A viruses. Shade represents high (dark green) vs. low (light green) relative growth in the growth assay (see panel C). **A.** Pairwise correlations between independent traits. **B.** Additional correlations that we hypothesized might occur ("mult. rate" multiplication rate; "rel. growth" relative growth). **A&B.** Each point represents one virus strain. Panels with significant Spearman correlations are marked with stars and a gray background. Note that the analyses were weighted by the precision of the retained estimates, and this weighting is not represented in the figure. A version of these panels with 95 % CIs can be found in Supp. Fig. S11. **C.** Results of the growth assay, expressed as an x-fold increase in virion concentration in 24 h. The 12 fastest-growing strains are marked.

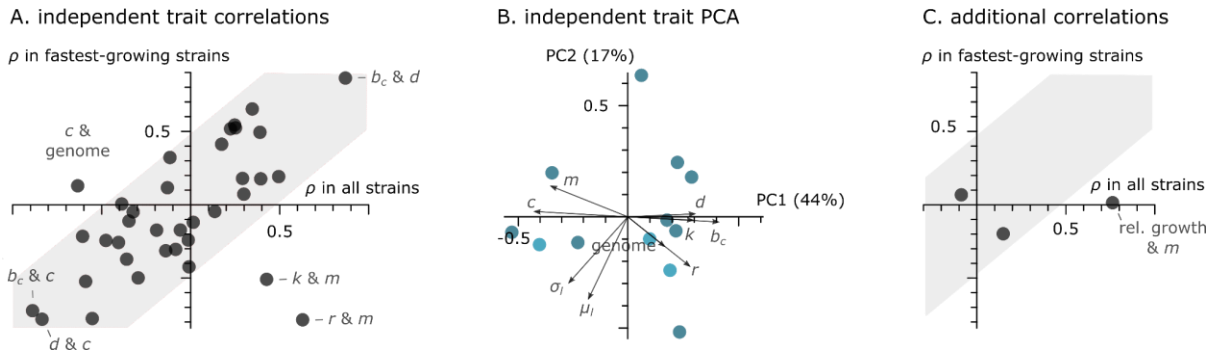

Fig. 5. Correlations between traits in the fastest-growing NC64A viruses. A&C. Comparison of Spearman's ρ correlation coefficients between independent traits (**A**) or for additional trait combinations (**C**) when all strains vs. the fastest-growing strains are used (see Fig. 4C). Each point represents one trait combination. The gray area marks the zone where $-0.5 \leq \Delta\rho \leq 0.5$; points outside this zone are labeled with the trait combination they represent. **B.** PCA of the independent traits in the fastest-growing strains. The biplot shown here was produced by the Ipca method; the PairCor result was extremely similar. The variance explained by each principal component (PC) is given on the axis. Each point represents one virus strain.

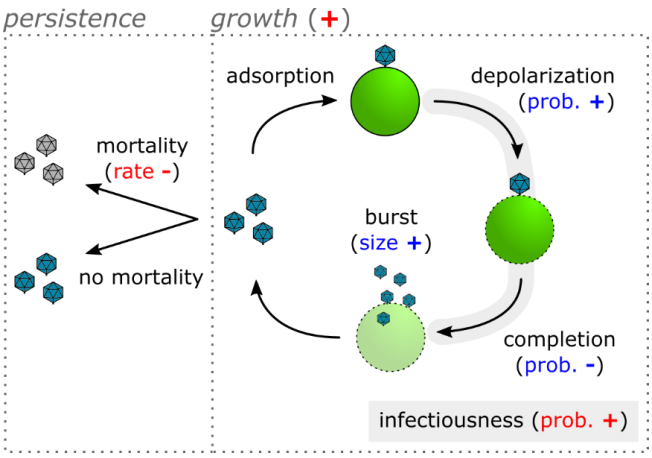

Fig. 6. Summary figure, showing a simplified life cycle and correlation results. The main life cycle steps (adsorption, depolarization, completion with burst, and decay) are shown, as well as relevant compound traits (specific infectivity, relative growth). In the NC64A viruses, there were two main correlational patterns that suggested life history trade-offs. The traits associated with these are marked in respectively blue and red.

951 **<u>Supplementary Material</u>**

952 Detailed legends provided in each file.

953 **Supplementary Method S1. Derivation of Eqs. 1 & 2.**

954 **Supplementary Table S1. Trait table for the chloroviruses, including selected traits from the**
955 **literature and the traits estimated in this manuscript.**

956 **Supplementary Table S2. ANOVA tables partitioning the trait variance within and among**
957 **chlorovirus groups.**

958 **Supplementary Table S3. Correlations between traits in the NC64A virus group.**

959 **Supp. Fig. S1. Example of statistical fitting for the mOSG model.**

960 **Supp. Fig. S2. Effect of imposing [illegible] = 0 in the mOSG model.**

961 **Supp. Fig. S3. Sensitivity of the mOSG model to its parameters.**

962 **Supp. Fig. S4. Repeatability of the mOSG assay.**

963 **Supp. Fig. S5. Effect of imposing *r* = 0 in the mP model.**

964 **Supp. Fig. S6. Sensitivity of the mP model to its parameters.**

965 **Supp. Fig. S7. Example of statistical fitting for the mP model.**

966 **Supp. Fig. S8. Repeatability of the mP assay.**

967 **Supp. Fig. S9. Correlations between model parameters arising from the fitting process.**

968 **Supp. Fig. S10. Effect of correlations between model parameters arising from the fitting process.**

969 **Supp. Fig. S11. Correlations between traits in the NC64A viruses, with 95 % CIs represented.**

970 **Supp. Fig. S12. Derivation of the independent traits *c* and b_c.**

971 **Supp. Fig. S13. Exploration of the assumption that mOSG parameters are independent of MOP.**